

The Influence of Water Saturation on the Nonlinear Elastic Mesoscopic Response in Earth Materials, and the Implications to the Mechanism of Nonlinearity.

K E-A. Van Den Abeele^a, J. Carmeliet^a, P.A. Johnson^b and B. Zinszner^c

^aLaboratory of Building Physics, Department of Civil Engineering, Catholic University Leuven, Celestijnenlaan 131, 3001 Heverlee, Belgium;

Koen.vandenabeele@bwk.kuleuven.ac.be ; Jan.Carmeliet@bwk.kuleuven.ac.be ;

^bEarth and Environmental Sciences Division EES-4, MS D443, Los Alamos National Laboratory, Los Alamos, NM 87545, USA; paj@lanl.gov ;

^cInstitut Français du Pétrole, B. P. 311-92506, Rueil-Malmaison Cedex, France; Bernard.Zinszner@ifp.fr .

ABSTRACT

Much is known empirically about the qualitative and quantitative nonlinear response of mesoscopic, porous media. As yet, however, the mechanism of nonlinear response in porous media is only speculation. In this work we illustrate evidence from several types of experiments indicating that fluid plays an important role in the nonlinear response. For instance, measurements at low degrees of water saturation indicate that molecular layers of adsorbed fluids as well as condensation fluids significantly influence the linear and nonlinear response at dynamic strain levels due to the activation of internal molecular forces. In rock, we observe a significant increase in the nonlinear response,

especially in the saturation range of 1-20%. This is consistent with the changes in the linear response, but the extent of the variation is larger in the nonlinear measurements, especially in rocks containing small pore systems. This is a result of an increased fluid-solid interaction upon wetting causing the material to expand and soften. Simultaneously, the micro- and mesoscopic hysteretic entities that cause the nonlinear response are activated at different pressures as a function of low saturation. As a consequence of the moisture induced forces, the amount of active hysteretic units increases with saturation. The fact that the nonlinear response increases with water saturation especially in the low saturation range , implies that the presence of moisture plays a major role in the nonlinear mechanism, or in the activation of that mechanism.

1. INTRODUCTION

Nonlinear response in Earth materials is very large, based on numerous observations from laboratory studies of rock [Johnson et al., 1996; Johnson and Rasolofosoan, 1996] and of unconsolidated sedimentary materials [e.g., Isihara, 1996, Hardin and Drnevich, 1972a, 1972b], and from field studies of nonlinearity in strong ground motion [e.g., Beresnev and Wen, 1996; Field et al., 1997]. More recently it has become clear that damaged solids (plastic, steel, etc.) also display very large nonlinear response, that can be qualitatively and quantitatively similar to Earth materials, despite the fact that their nonlinear response is highly localized rather than volumetric, as in Earth materials. It has been suggested that materials exhibiting similar levels of nonlinear behavior form a class of materials, the

Nonlinear Mesoscopic Elasticity Class [Guyer and Johnson, 1999], that can be described by the Preisach-Mayergosz space theory of nonlinear elasticity [Guyer et al., 1994, 1995, 1997; McCall and Guyer, 1994]. In contrast, materials with *Atomic Elasticity* have a small nonlinear response, which is due entirely to their atomic anharmonicity. These are classical nonlinear materials including undamaged individual crystals, many fluids, metals without dislocations, plastics, etc., that can be described by classical Landau theory [e.g., Hamilton, 1986; Naugolnykh and Ostrovsky 1998]. Based on our experience, it appears that all of the materials in the nonlinear mesoscopic elasticity class have low-aspect ratio features in common (microcracks, macrocracks, grain-to-grain contacts), making them more compressible than atomic elastic materials, and leading, in some manner or another, to a larger nonlinear response.

It is well known that at large strain levels, friction between constituents is one of the important mechanisms which contributes to the extreme nonlinearity of porous materials [Dreyer, 1972]. However, a lower limit of nonlinear behavior has not been observed [TenCate and Shankland, 1998], even at strains of 10^{-9} and displacements approaching atomic dimension, where it is unlikely that mechanical frictional effects take place.

Low-aspect ratio features and micro-inhomogeneous imperfections can be conduits for moisture. Fluids can change the linear behavior of mesoscopic materials in well-known, dramatic manners. Especially in the low saturation range where molecular adsorption and capillary condensation (formation of menisci) occurs, a significant decrease of elastic moduli is observed in porous media [e.g., Bourbié et al., 1986]. It is not unreasonable to hypothesize that a similar effect may persist and govern the

nonlinearity of wetted pore surfaces and contacts in porous materials. Indeed, it is well-known in Atomic Force Microscopy that the presence of moisture can produce nonlinear and hysteretic effects between the probe and a wetted surface [Binggeli and Mate, 1995; Capella and Dietler, 1999].

Thus we have evidence suggesting that, (1) nonlinearity is related to micro-, meso-, and macrostructural features; (2) linear elastic behavior in mesoscopic porous solids can be greatly influenced by the presence of fluids; (3) nonlinear and hysteretic surface forces associated with wetting are widely observed; and (4) a limit to the nonlinear response is not observed, even at the very smallest strains measured ($\sim 10^{-9}$) where mechanical frictional effects are absent. Taken as a whole, these observations imply that the role of fluids must be important in the nonlinear behavior of mesoscopic materials.

The focus of the work presented here is to investigate in greater detail the influence of fluids on the linear and nonlinear response of rock, and to draw conclusions from these observations. First, we will illustrate linear and nonlinear dynamic properties in the range of 0.1% to +99% water saturation taken from two different rock types (two sandstones and one limestone). We will also show evidence from quasi-static tests taken at near zero and near 100% water saturation. In a second section, we focus on a combined theoretical and experimental prediction of the microstructural fluid-solid interaction forces that are involved in the saturation process. To this extent, we first define the dominant moisture induced forces at the microscopic level, and the equivalent macroscopic force assuming thermodynamical and mechanical equilibrium conditions. Then, we measure the saturation as function of the capillary pressure, which is the chemical pressure difference between the phases of liquid water and mixed water vapor with dry air at the

meniscus. In the third stage, we express the linear and nonlinear measurements in terms of the chemical pressure. This allows us to delineate the range of microstresses where the moisture induced activation of the linear and nonlinear properties is most pronounced. That is, are capillary forces more important than molecular adsorption forces, for instance. As a final topic in the discussion, we put the observations in perspective to the phenomenological PM-space model of McCall and Guyer (1994) for the description of nonlinear quasi-static and dynamic behavior of hysteretic media.

2. LINEAR AND NONLINEAR PROPERTIES VERSUS SATURATION

In this section, we report on the dynamic and quasi-static experiments and results at various saturation levels.

2.1. Experiments

Two types of experiments are performed: dynamic and quasi-static experiments. We use the resonance method for extracting the dynamic linear and nonlinear behavior of three rock samples. The nonlinearity is quantified by studying the resonance frequency shift of the fundamental mode as a function of drive level [e.g., Johnson et al, 1996; Zinszner et al, 1997; TenCate and Shankland, 1998; Van Den Abeele et al., 2000]. The quasi-static measurements were made in a pressure vessel at two saturation states (dry and fully saturated), using the resonance method as well [Zinszner et al, 1997].

Rock samples. Two different rock types with very different internal structure were studied: Lavoux limestone and Berea and Meule sandstone. The limestone is a pelletoidal rock, composed of 99% calcium carbonate (calcite). Meule and Berea sandstone are composed of quartz grains and contain a considerable amount of clay and other secondary mineralization. The bonding material is primarily silica. Physical properties and dimensions of these rocks are shown in Table 1.

Dynamic Resonance Measurements. The basic elements of the experimental configuration for obtaining frequency versus acceleration measurements are shown in Figure 1. A frequency sweep interval is chosen to encompass frequencies well above and well below the fundamental resonance mode of the sample. For cylindrical samples (Lavoux and Meule) we studied the lowest order longitudinal mode. The Berea sandstone samples were cut into beams (elongated rectangular parallelepiped), and the study was conducted on the lowest order bending mode. The samples are excited either by an electromagnetic (coil/magnet), piezoelectric, or shaker-type source affixed to the sample (longitudinal mode study), or by a non-contact speaker coupled through air (flexural mode study). At each frequency of excitation, the response signal is detected by a calibrated accelerometer and analyzed to obtain amplitude and phase of the input frequency wave. The input is stepped through the frequency band of interest, and the acceleration amplitude (output) is recorded as function of the drive frequency. Typically, 5-20 stepped sine experiments are conducted at successively increasing drive voltages over the same frequency interval in order to monitor resonant peak shift and harmonic generation for extraction of the nonlinear response. Time-series signals are captured as well for Fourier analysis.

Measurements were taken at numerous water saturation levels between approximately 0.1-99%. For Lavoux and Meule, the samples were 100% saturated after oven drying and then saturating under vacuum. Measurements were made as the rock slowly dried under room conditions, ensuring a uniform moisture distribution over the specimen. For Berea, the measurements started at the capillary water saturation level (free imbibition). Densities were derived from the dry and wet weights [Bourbie et al, 1986].

Quasi-Static Measurements. The resonant bar pressure vessel is described by Lucet et al. (1991) and Zinszner et al. (1997). In order to perform measurements under effective pressure, the bar is jacketed and sealed. (Effective pressure is the confining pressure minus the pore pressure.) The pore pressure is assumed to be in equilibrium with the atmosphere. The bar is supported in the center to avoid clamping effects on the fundamental resonant mode. A source and a detector are affixed to the sample, similar to the experiments at ambient conditions. The small mass loading effects [Lucet et al., 1991] are not accounted for because we are studying relative, not absolute, changes. Low excitation (linear) resonance measurements are performed inside the vessel in the same manner as described above.

The linear properties (elastic modulus and attenuation) of Lavoux and Meule samples were studied under different effective pressures at two states of fluid saturation. First, measurements were made in the dry state after oven drying at 70^o C. Measurements were also made at 100% tap water saturation.

In all of the above experiments, comparative studies were conducted using atomic elastic standards (aluminum, PVC, Plexiglas, Pyrex glass, etc.) to be certain that the apparatus was not contributing to the nonlinearity.

Measurements: The linear Q (inverse attenuation) is obtained in the standard manner from the halfwidth at half maximum of the resonance peak at low excitation. The linear Young's modulus (E) is calculated from the resonance frequency peak and the measured density (ρ) at each saturation level:

$$E=(2Lf_0)^2 \rho \quad \text{for cylindrical samples} \quad (1a)$$

$$E=\left(\frac{8\sqrt{12}}{\pi} \frac{L}{d} \left(\frac{L}{3.0122}\right)^2 f_0\right)^2 \rho \quad \text{for strips} \quad (1b)$$

where L is sample length, d its thickness (for strips) and f_0 the resonance frequency.

The nonlinearity property is derived from the change in resonance frequency with calculated strain amplitude (ϵ) normalized to the linear resonance frequency: $(f_0-f(\epsilon))/f_0$ [see, e.g., Van Den Abeele et al., 2000]. In short, the change in frequency represents the softening of the modulus induced by wave excitation, which is one measure of the nonlinear response. Strain amplitude (ϵ) is calculated from the measured acceleration amplitude (A) in the following manner:

$$\varepsilon = \frac{A}{4\pi L f^2} \quad \text{for cylindrical samples} \quad (2a)$$

$$\varepsilon = \frac{0.219}{f^2} \frac{\pi}{8} \frac{d}{\sqrt{12}} \left(\frac{3.0112}{L}\right)^2 A \quad \text{for strips.} \quad (2b)$$

At all saturation levels, we found a ubiquitous linear decrease of the resonance frequency as function of the strain amplitude. The proportionality coefficient “ α ” relating the relative frequency shift to the strain amplitude is used to quantify the nonlinearity:

$$\frac{\Delta f(\varepsilon)}{f_0} = \frac{f_0 - f(\varepsilon)}{f_0} = \alpha \varepsilon \quad . \quad (3)$$

It is well known that the proportionality coefficient α is a measure of the dynamic stress-strain hysteresis [Guyer et al., 1994, 1995; McCall and Guyer, 1994; Van Den Abeele et al., 1997, 2000]. We assume here that the nature of the nonlinearity is merely hysteretic, and not “classical atomic”. Based on the P-M space theory and the measurements to follow, this is a reasonable assumption.

In the following we discuss the evolution of the inverse attenuation (Q), the linear modulus (E) and the dynamic hysteresis coefficient (α) as function of saturation (S) for Lavoux, Meule and Berea.

2.2. Results

Limestone. The linear modulus E and inverse attenuation Q for Lavoux limestone are shown in Figure 2. These are typical changes of the linear dynamic properties with saturation [e.g., Bourbié et al., 1986]. We see a moderate change in the linear modulus of approximately 15% from 0.1% to 70% water saturation. Over the same saturation interval, the quality factor Q decreases by about 95%. In Figure 3, the nonlinear response is illustrated as function of saturation: Figure 3a shows a subset of the actual measured values of the relative frequency shift (Eq.(3)) as function of the inferred strain at different saturation levels. The evolution of the nonlinearity coefficient α is shown in Figure 3b. There is a clear progression from less to more nonlinear as saturation increases from 0.1% to 31%, changing by one order of magnitude. Above this saturation level, the nonlinear response remains approximately the same up to the highest saturation. Note that the change in linear velocity with saturation, as observed in Figure 2, is eliminated by normalizing to f_0 (as in Eq.(3)).

Sandstone. The linear Young's modulus as a function of saturation is shown in Figure 4 for Meule and Berea (the Q response was not measured). Between 0 and 20%, we see a much larger change in linear modulus with saturation than in the limestone. The modulus changes very little beyond approximately 20-25% saturation. These are common observations between sandstone and limestone, and are generally attributed to the different type of pore space geometry [see e.g., Lucet et al., 1991; Bourbié et al., 1986]. Figure 5 shows the nonlinear response of the two sandstones as a function of saturation, quantified in terms of the above defined hysteretic nonlinearity coefficient. We observe

once again an initial sharp increase in the nonlinear response with water saturation. The maximum nonlinearity is observed in the range of 8-16% water saturation, whereupon the nonlinear response decreases gradually with saturation.

Quasi-Static Results. In a qualitative manner, the quasi-static results for dry conditions and at full saturation, shown in Figure 6, support the above observations. Figure 6a illustrates that the linear velocity (equivalently modulus) for Lavoux under dry conditions changes very little as a function of effective pressure, whereas the material becomes more nonlinear and much more hysteretic at full saturation. The measurements made on Meule sandstone (Figure 6b) show that the material behaves more nonlinearly at full saturation as well (44% change in the 0-40 Mpa pressure range versus 24% for dry conditions). In Figure 7, we plot the relative change in linear, longitudinal velocity under 100% saturation conditions versus the change in longitudinal velocity under oven-dry conditions measured at the same pressure levels. For Meule (Figure 7b), the dependence reveals that the nonlinearity has increased by a constant factor 2 over the entire pressure range. For Lavoux (Figure 7a), we obtained a steeper increase at low pressures (factor 8) than at high pressures (factor 4). The factors 2 (for Meule) and 8 (for Lavoux) are in excellent quantitative agreement with the dynamic observations of the nonlinearity coefficients at these saturation levels performed under ambient pressure conditions. Indeed, in Figure 5 we note an increase in nonlinearity from 2500 to 5000, and in Figure 3b α changes from 500 to 4000.

In the above experiments, the nonlinear response of the rock samples changes significantly with saturation, in particular, between 0% and 10-25% water saturation. At the same time, there is a notable change in the linear properties such as dissipation and wavespeed. Clearly, there are connections between the influence of water saturation on the mechanism of nonlinear and linear elastic behavior. In the next section we express and analyze the above observations in the context of the internal forces induced by the presence of moisture.

3. MOISTURE INDUCED MICRO-FORCES

Because rocks are hydrophilic materials and contain a huge specific (internal) surface area due to pore space, they exhibit intense fluid-matrix interactions because of molecular and surface forces. The induced forces are known to be extremely sensitive to fluid saturation level [e.g., Carmeliet *et al.*, 1999]. Solid-fluid pressures include molecular adsorption forces along pore walls, capillary pressures in capillary pores, and interlayer fluid pressures due to the presence of interlayer hydrate water in nanopores. As a convention, we assume that positive pressures correspond to tensile loading, and negative pressures to compression.

In the following we will illustrate and discuss the relation between the linear and nonlinear elastic phenomena and the moisture induced forces which are present as function of the saturation. First, we identify the various moisture induced forces at the microscopic level. Next, we interpret the global influence of the microscopic forces on a macroscopic level and establish the link between the equivalent macroscopic force and

the level of saturation. Using these results, we relate the effective influence of the microscopic forces on a macroscopic level to the observed moisture dependence of the linear and nonlinear elastic properties of the two rocktypes.

3.1. Moisture Induced Forces at the Microscopic Scale

At very low saturation levels, the adsorption process is governed by the interaction of repulsive and attractive forces between the water molecules and the molecules or ions of the solid. Water adsorption is a consequence of the larger molecular attraction forces of water molecules to the solid than the binding forces of gas molecules to the solid [Israelachvili, 1985]. Upon balancing the forces, the layers of adsorbed water on the pore walls exposed to water vapour are subjected to a microscopic *spreading pressure*, which reduces the surface tension of the solid. This spreading pressure decreases with increasing distance from the solid wall.

At higher levels of saturation, capillary condensation takes place. Capillary condensation commences when the molecular adsorbed water layers in the finest pores abruptly alter to a more stable arrangement, due to surface tension, by forming a meniscus between the liquid water (l) and gas phase (g) (Figure 8). As one may expect, this sudden transition does not occur uniformly over the entire sample. It is highly dependent on the range of pore dimensions inherent to rocks. Under certain restricted conditions (isothermal, no salts, ...), the chemical potential governing the capillary condensation process can be expressed in terms of the microscopic *capillary pressure*, π_c , which is defined as the difference between the pressure in gaseous and liquid phases across the meniscus:

$$\pi_c = \pi_g - \pi_l \quad (4)$$

Kelvin's law, which relates the microscopic capillary pressure π_c to the pore relative humidity RH above the meniscus, states that isothermal thermodynamic equilibrium at the meniscus occurs when

$$\ln(RH) = -\frac{\pi_c}{\rho_l R_v T} \quad (5)$$

with RH the relative humidity, π_c the capillary pressure, ρ_l the density of liquid water (1000 kg/m³), R_v the universal gas constant for water vapour (462 J/KgK) and T the room temperature (293 K).

Since the microscopic capillary pressure π_c (in absence of external loads) is always positive, it exerts a tensile loading on the pore water leading to a compressive microscopic reaction pressure π_c^R in the solid (Figure 9a). According to Kelvin's law (Eq.(5)) the microscopic capillary pressure is a decreasing function of the relative humidity (e.g. at RH=0.4 (25°C), π_c =124 MPa, and at RH=0.9, π_c =14 Mpa).

In a very fine pore system, it is possible that the full thickness of the adsorption layers cannot develop for a given RH, and that water adsorption is hindered. A microscopic *swelling pressure*, π_s , arises as a result of repulsion forces between water molecules, keeping the pore walls at a certain distance [Powers, 1965; Wittmann, 1974; Bazant, 1970]. Bazant shows that the swelling pressure can be extremely high. For

example, in a pore that is only two water molecules thick, $\pi_s=174$ MPa at $RH\approx 1$. Typical examples of such fine pore structures can be found in media which are rich in clays and CSH (Calcium-Silicate-Hydrate) particles, composed of laminar sheets with interlayer adsorbed water. The repulsive forces at the solid surfaces drive the laminar sheets apart and the cohesive forces between the solid walls decrease. The net result is a microscopic compressive force of the adsorbed water on the solid. These microcompressive liquid forces are balanced by tensile microforces π_s^R in the solid (Figure 9b). Although no thermodynamical proof exists and the microscopic swelling pressure has never been measured as function of RH, π_s is generally considered to be dependent on the relative humidity according to a Kelvin type law [Bazant *et al.*, 1997]

$$\pi_s = -C_1 \rho_l R_v T \ln(RH) + C_2 \quad (6)$$

where C_1 and C_2 are weak functions of the RH (constants in a first approximation, $C_1 > 0$).

In summary, the microscopic capillary pressure (always positive) decreases with increasing degree of saturation, which results in a decrease of the compressive reactive microstresses in the solid. The microscopic swelling pressure (always negative) increases in absolute value with increasing degree of saturation, giving rise to increasing microscopic tensile reaction forces in the solid. When microscopic capillary pressures are dominant, the solid material will sustain compressive microscopic forces. When swelling pressures prevail, the material matrix will experience tensile microstresses. Without making further assumptions about the real dependence of the swelling pressure on RH,

we may assume that the net microscopic reaction pressure effect results in either compressive or tensile loading of the solid. As saturation increases, the reactive loading of the solid will evolve from a compressive to a less compressive or even a tensile loading, and from a low tensile loading towards a more extreme tensile loading of the solid (Figure 10).

3.2. Equivalent Macroscopic Forces and State Relation

We now assume that all pore water in the microstructure is locally in thermodynamic equilibrium. Therefore, changes in microscopic capillary pressure will almost instantly result in changes of microscopic swelling pressure and interlayer water pressure. The net result of all moisture induced microstresses on the liquid can then be expressed at the macroscale by one macroscopic liquid pressure p_l . This macroscopic liquid pressure can be seen as the average result of all the microscopic pressures acting at the pore scale. Assuming the gaseous phase in thermodynamic equilibrium with the outside (p_g at constant atmospheric pressure) the macroscopic liquid pressure p_l can be replaced by the macroscopic capillary pressure p_c ($p_c = p_g - p_l$), which is commonly used in fluid transport modeling [Bear and Bachmat, 1991]. In this context, the macroscopic capillary pressure can be considered to be representative of the combined effects of all complex microscopic fluid-solid interaction forces.

The relation between the degree of saturation S and macroscopic capillary pressure p_c is referred to as the capillary pressure curve: $S(p_c)$. In order to obtain the capillary pressure (or water retention) curves, we performed mercury intrusion experiments on all three rocks in addition to measurements of adsorption isotherms [for

details, see Clyde, 1969; Van Brakel et al., 1981]. The experimentally obtained state relation can be fit in an analytical form by a sum of power functions [Carmeliet et al., 1999]

$$w(p_c) = w_{sat} \sum_{i=1}^k l_i \left(1 + (c_i p_c)^{n_i} \right)^{1 - \frac{1}{n_i}} \quad (7)$$

where k is the number of power functions and l_i are the weighting factors ($0 < l_i \leq 1$, $\sum l_i = 1$). The fully saturated moisture content w_{sat} is defined as the moisture content upon complete filling of the open porosity with water. This value can be determined in a separate vacuum saturation experiment. The analytic approximations of the water retention curves obtained by fitting the measurement data to Eq.(7) for the three different rocks (Berea, Meule and Lavoux, normalized to the respective w_{sat} values) are illustrated in Figure 11. The fitting parameters are summarized in Table 2. There is a clear difference between Lavoux Limestone and the two sandstones. At saturation levels of 25% and more, the limestone is subjected to much higher internal forces.

3.3 Implications of moisture on dynamic properties

Range of moisture influenced dynamics. Now that we have quantified the state relation $S(p_c)$, we can express the measured linear and nonlinear parameters as a function of the equivalent macroscopic capillary pressure. Figure 12 shows that the primary changes in the linear and nonlinear parameters are restricted to small ranges of capillary pressures. In terms of relative humidity, the changes occur in range 0.8 to 0.9975 RH, where the microscopic capillary pressures and swelling pressures prevail, and the microscopic adsorption forces are of less importance. It's remarkable that the nonlinear coefficients for Berea and Meule decrease again at lower capillary pressures.

Macroscopic implications. The perception of moisture induced microforces has some interesting implications, which are in agreement with the observations. 1) The decrease of compressive microloading with the degree of saturation obviously results in a reduction of the stiffness property of the material. 2) At the same time, the mobility of the constituent particles increases, and likewise the number of nonlinear and/or hysteretic micro-inhomogeneities (grain-to-grain boundaries, asperities, microcracks, etc., also termed hysteretic mesoscopic unit, HMU, see later) and their ability to change states (contact-no contact; open-close; pin-unpin) increases with the degree of saturation. Therefore, an increase of nonlinear elastic effects is expected. 3) At complete saturation (98% and up) the apparent stiffness of the wet material can increase again due to the stiffening effect of the water, which acts as a one phase solid material sustaining part of the external load. 4) From XRD-analysis (Table 1) and thin section analysis (not illustrated), we know that both Meule and Berea sandstone have at least some percentage

of clays and CSH particles, and must be sensitive to swelling pressures. The effect of the swelling pressure can lead to an extreme tensile microloading, which may inactivate micro-inhomogeneities and exclude them from contributing to the macroscopic nonlinear behavior of the material, resulting in a reduction of the nonlinearity parameter. It is expected that Lavoux Limestone is less sensitive because of its nearly pure composition of Calcite. In this case, a saturation of the macroscopically observed nonlinearity is expected. 5) Finally, the increasing swelling pressure with saturation may explain in a part the observed reduction of the tensile strength of a material at higher degrees of saturation (an observation that is not shown here, but is well known in literature, e.g. Hiller (1964)).

Implications for P-M space modeling. As a final remark, we link our observations to the current state-of-the-art model that is used to describe static and dynamic nonlinear behavior in rock-type materials. Based on the work of F. Preisach and I. Mayergoyz, Guyer and McCall have developed a phenomenological model to describe the quasistatic stress-strain relation in rocks [Guyer et al., 1994, 1995, 1997; McCall and Guyer, 1994]. In this model, called the P-M space model, a rock is represented as an assemblage of elastic elements that behave either reversibly or hysteretically as function of the externally applied stress σ . A hysteretic element, also called HMU (hysteretic mesoscopic unit), can be in only one of two states, open or closed. The behavior of a single HMU is such that it is originally open with length L_0 , closes to length L_c as the applied stress increases to σ_c , and remains closed as the stress continues to increase. When the applied stress is decreased, the element opens at σ_0 (different from σ_c), changing back to its original

length L_0 , and remaining there as stress decreases further (Figure 13a). A large number of such elements with differing L_0 , σ_0 , L_c , and σ_c models the heterogeneous elastic elements of the rock's bond system. A reversible element is an element with identical closing and opening pressures.

The stresses σ_0 and σ_c for each element can be used as the element's coordinates in "P-M space", thus creating a density of elements in the σ_0 - σ_c space (with $\sigma_0 \leq \sigma_c$). An academic example is shown in Figure 13b. Reversible elements reside on the diagonal of the σ_0 - σ_c space. Hysteretic elements fill the space $\sigma_0 < \sigma_c$. As the stress on the rock is varied, one can use P-M space to keep track of which elements are open and which are closed, and simulate the stress-strain response of the rock.

In a dynamic experiment, e.g. sinusoidal cycling between $\bar{\sigma} - \Delta\sigma$ and $\bar{\sigma} + \Delta\sigma$ ($\bar{\sigma}$ being the ambient external stress, and $\Delta\sigma$ the maximum stress excursion), one samples only a small triangle in P-M space. The dynamic properties of a material can be probed by studying the density within the triangle [Guyer et al., 1994, 1995; McCall and Guyer, 1994; Van Den Abeele et al., 1997]. Elements outside this "activation triangle" are left untouched. A quasi-analytical treatment of P-M space reveals that the elements on the diagonal control the linear modulus of the material: the more elements on the diagonal, the softer the material (increase of compliance). The number of off-diagonal or hysteretic elements determine the amount of hysteretic nonlinearity: the more elements off the diagonal, the larger the nonlinearity. Thus, on the one hand, the observed decrease of the stiffness with increasing saturation can be translated to an increase of the reversible elements. At the same time, the observed increase of nonlinearity implies that the density of hysteretic elements within the probed region in P-M space increases as well. These

implications are illustrated in Figure 14. Due to the net extension of the solid matrix with saturation (decrease of internal compression forces or increase of tension) as a result of an increased fluid-loading, the same excursion in external stresses in a wet state will be able to activate more units than in a dry state, resulting in a larger density of HMU's in the activation triangle, and therefore a higher nonlinearity. This means that partial saturation induces a shift in the distribution of the elastic elements in the P-M space towards a higher (external) stress range. The total number of elastic elements in P-M space is assumed conserved. Only the number of activated units increases with saturation. We are currently attempting to substantiate and quantify the shift of the HMU's by conducting static stress-strain measurements on rock samples at various levels of saturation [Carmeliet and Van Den Abeele, 2000].

4. CONCLUSIONS

The experiments we described in this paper suggest evidence for the role of fluids on the nonlinear behavior of two rock-types: pelletoidal limestone (Lavoux) and clay rich sandstones (Meule and Berea). We conducted both quasi static and dynamic measurements. In the quasi-static experiments we measured Young's mode resonance as a function of confining pressure on saturated and dry samples. In the dynamic measurements we applied Young's mode resonance on samples at ambient temperature and pressure conditions as a function of saturation from approximately 0.1% to 99% saturation. The nonlinear response is extremely sensitive to the water saturation, especially at low saturation (<10-20%). The relative increase in nonlinearity for dry and

fully saturated samples, measured by both the quasi-static and the dynamic experiments described here, are in very good agreement.

From a macroscopic perspective, at low water saturation the microscopic fluid-solid interactions result in a prestressing of the solid. As saturation increases, the compressive microstresses decreases, leading to an expansion of the solid matrix. Due to this expansion, the dynamic mobility of the material's mesoscopic entities increases with saturation, and a reduction of the stiffness together with an increase in damping of the material can be expected. At the same time the number of active nonlinear and/or hysteretic micro-inhomogeneities (grain-to-grain boundaries, asperities, microcracks, etc.) and their ability to change states (contact – no-contact; open-close; pin-unpin) increases with the degree of saturation. Therefore, an increase of nonlinear elastic effects is expected at low saturation (<10-20%). At larger saturations (>20%), the effect of the microstresses levels off. In clay-rich materials, the capillary pressure can be countered by an extreme swelling pressure, and the nonlinearity may decrease as a result of locking due to the tensile microstresses that are induced.

In terms of modeling implications, we showed that the moisture induced effects can be interpreted as a relocation in the density of HMU's in the P-M space, which represents the (linear and nonlinear) elastic behavior of the rock's bond system. The observed decrease of the stiffness with increasing saturation can be interpreted as an increase of the reversible elements. At the same time, the increase of nonlinearity points towards an increase of the number of hysteretic elements near, but not on, the P-M space diagonal.

ACKNOWLEDGMENTS

This work was performed under the auspices of the Flemish Institute for the Advancement of Science and Technology in Industry, the Flemish Fund for Scientific Research, the Research Council of the Catholic University of Leuven, Belgium, and the Office of Basic Energy Research, Engineering and Geoscience (contract W-7405-ENG-36), US Department of Energy with the University of California.. The authors also acknowledge support by a University Collaborative Research Program of The Institute of Geophysics and Planetary Physics at Los Alamos National Laboratory, NM, USA. Work was also supported in part by the Institut Français du Pétrole, Rueil-Malmaison, France. We are indebted to R.A. Guyer for valuable suggestions and to M. Masson for experimental assistance.

Received _____

Copyright 1999 by the American Geophysical Union.

REFERENCES

- Bazant Z.P., Constitutive equation for concrete creep and shrinkage based on thermodynamics of multi-phase systems, *Mat. and Struct.*, Paris, France, 3, 3-36, 1970.
- Bazant Z.P., A.B. Hauggaard, S. Baweja, and F-J. Ulm, Microprestress-solidification theory for concrete creep. I: Aging and Drying effects, *ASCE J. Eng. Mech.*, 1188-1194, 1997.
- Bear, J. and Y. Bachmat, *Introduction to modeling of transport phenomena in porous media*, Kluwer Academic Publishers, Dordrecht, 1991.
- Beresnev, I.A. and K.-L. Wen., Nonlinear soil response- a reality?, *Bull. Seism. Soc. Am.* 86, 1964-1978, 1996.
- Binggeli, M. and C.M. Mate, Influence of Water Vapor on Nanotribology Studied by Friction Force Microscopy, *jvst*, B13, 1312-15, 1995.
- Bourbié, T, O. Coussy, and B. Zinszner, *Acoustique des milieux poreux*, Editions Technip, Paris, 1986.
- Capella, B. and G. Dietler, Force-distance curves by atomic force microscopy, *Surface Science Reports*, Vol 34, Nos. 1-3, 1999, pp. 1-104, 1999.
- Carmeliet, J., G. Houvenaghel, and F. Descamps, Multiscale network for simulating liquid water and water vapour transfer properties of porous materials. *Transport in Porous materials*, 35: 67-88, 1999.
- Carmeliet J. and K.E.A. Van Den Abeele, in preparation, 2000
- Clyde Orr, Jr., Application of Mercury Penetration to Materials Analysis, *Powder Technology*, 3, pp.117-123, 1969/70.

- Dreyer, W., *The science of rock mechanics. 1: The strength properties of rocks*, :Series on rock and soil mechanics, (Trans Tech publ. Clausthal), 1972.
- Field E.H., P.A. Johnson, I. Beresnev, and Y Zeng, Nonlinear ground-motion amplification by sediments during the 1994 Northridge earthquake, *Nature*, 390, 599-602, 1997.
- Guyer, R. A., K. R. McCall, and G. N. Boitnott, Hysteresis, discrete memory and nonlinear wave propagation in rock, *Phys. Rev. Let.*, 74, 3491-3494, 1994.
- Guyer, R. A., K. R. McCall, P. A. Johnson, P. N. J. Rasolofosaon, and B. Zinszner, Equation of state hysteresis and resonant bar measurements on rock, International Symposium on Rock Mechanics, J. J. K. Daemon and R. A. Schultz, Eds., Balkema, Rotterdam, 177-181, 1995.
- Guyer, R. A., K. R. McCall, G. N. Boitnott, L.B. Hilbert Jr., and T.J. Plona, Quantitative implementation of Preisach-Mayergoyz space to find static and dynamic elastic moduli in rock, *J. Geophys. Res.*, 102, 5281-5293, 1997.
- Guyer, R.A., and P.A. Johnson, Nonlinear mesoscopic elasticity: Evidence of a new class of materials, *Physics Today* 52, 30-35, 1999.
- Hamilton, M. F., Fundamentals and applications of nonlinear acoustics, in *Nonlinear wave propagation in mechanics -- AMD-77*, The American Society of Mechanical Engineers, New York, 1986.
- Hardin B.O., and V.P. Drnevich, Shear modulus and damping in soils: measurement and parameter effects, *J. Soil Mech. Foundations Div. ASCE* 98, 603-624, 1972a.
- Hardin B.O., and V.P. Drnevich, Shear modulus and damping in soils: design equations and curves, *J. Soil Mech. Foundations Div. ASCE* 98, 667-692, 1972b.

- Hiller, K.H., Strength reduction and length changes in porous glass caused by water vapour adsorption, *J.Appl.Phys.* 35(5), 1622-1628, 1964.
- Isihara, K., *Soil behavior in earthquake geotechnics*, Clarendon Press (Oxford University Press) New York, 1996.
- Israelachvili, *Intermolecular and Surface forces with application to colloidal and Biological Systems*, Academic Press, London, 1985.
- Johnson, P. A., B. Zinszner, and P. N. J. Rasolofosaon, Resonance and nonlinear elastic phenomena in rock, *J. Geophys. Res.*, 101, 11553-11564, 1996.
- Johnson, P. A and P. N. J. Rasolofosaon, Manifestation of nonlinear elasticity in rock: convincing evidence over large frequency and strain intervals from laboratory studies, *Nonlinear Processes in Geophysics* 3, 77-88, 1996.
- Lucet, N., P. N. J. Rasolofosaon, and B. Zinszner, Sonic properties of rock under confining pressure using the resonant bar technique, *J. Acoust. Soc. Am.* 89, 980-990, 1991.
- McCall, K. R. and R. A. Guyer, Equation of state and wave propagation in hysteretic nonlinear elastic material, *J. Geophys. Res.* 99, 23,887-23,897, 1994.
- Naugolnykh, K., and L. Ostrovsky, *Nonlinear Wave processes in Acoustics*, Cambridge Texts in Applied Mathematics, Cambridge University Press, 1998.
- Powers, T.C., Mechanism of shrinkage and reversible creep of hardened cement paste. Proc. Int. Conf.on the Struct. of Concrete, Cement and Concrete Association, London, U.K., 319-344, 1965.

- TenCate, J. and T. J. Shankland, Slow dynamics and nonlinear response at low strains in Berea sandstone, Proc. 16th Intl. Congress on Acoust., Eds. P. Kuhl and L. Crum, Seattle, Washington, v.3, 1563-1566, 1998.
- Van Brakel, Modry & Svata, Mercury Porosimetry: State of the Art, Powder Technology 29, pp. 1-12, 1981.
- Van Den Abeele, K. E-A., P. A. Johnson, R. A. Guyer, and K. R. McCall, On the analytical solution of hysteretic nonlinear response in elastic wave propagation, *J. Acoust. Soc. Am* 101, 1885-1898, 1997.
- Van Den Abeele, K. E-A., J. Carmeliet, J.A. Ten Cate, and P. A. Johnson, Nonlinear Elastic Wave Spectroscopy (NEWS) techniques to discern material damage. Part II: Single Mode Nonlinear Resonant Acoustic Spectroscopy (SIMONRAS), Res. Nondestr. Eval. in press, 2000.
- Wittmann F.H., Bestimmung physikalischer Eigenschaften des Zementsteins. Deutscher Ausschuss für Stahlbeton, Heft 232, W. Ernst & Sohn, Berlin, Germany, 1-63 (in German), 1974.
- Zinsner, B., P.A. Johnson, and P.N.J. Rasolofosaon, Influence of change in physical state on elastic nonlinear response in rock: effects of confining pressure and saturation, *J. Geophys. Res.* 102, 8105-8120, 1997.

FIGURE CAPTIONS

Figure 1: Basic elements of a Resonant Bar Experiment

Figure 2: Young's Modulus E (a) and Inverse attenuation Q (b) as function of saturation for Lavoux limestone.

Figure 3: Changes in nonlinear response as function of saturation for Lavoux limestone.

a) Relative Resonance Frequency Shift versus inferred strain for different saturation levels.

b) Inferred Hysteretic Nonlinearity Coefficient α as function of saturation.

Figure 4: Young's Modulus E as function of saturation for Meule and Berea Sandstone.

Figure 5: Inferred Hysteretic Nonlinearity Coefficient α as function of saturation for Meule and Berea sandstone.

Figure 6: Quasi-static velocity measurements as function of pressure for oven-dry and 100% water saturated samples of Lavoux (a) and Meule (b) (From Zinszner et al., 1997).

Figure7: Relative change in longitudinal velocity under 100% saturation conditions versus the relative change in longitudinal velocity under oven-dry conditions measured at the same pressure levels for Lavoux (a) and Meule(b). Due to the extreme hysteresis observed in the saturated Lavoux data, we used the mean of the interpolated velocities at each pressure level. For Lavoux a steep relation at

low pressures (factor 8) is followed by moderate proportionality at high pressures (factor 4). For Meule, the dependence reveals that the nonlinearity has increased on average by a factor 2 over the entire pressure range.

Figure 8: Sorption processes: Adsorption and Capillary Condensation

Figure 9: Moisture induced microforces: capillary (a) and swelling pressure (b) induce competing microscopic matrix reaction.

Figure 10: Solid matrix reaction due to microscopic capillary and swelling pressures. If the microscopic swelling pressure is important (e.g., in materials with clays and CSH-particles), this can lead to an extreme tensile matrix reaction near $RH=1$. This effect is highly exaggerated in this figure for illustrative purposes.

Figure 11: Capillary pressure (water retention) curves of Lavoux limestone and Meule and Berea Sandstone, measured by mercury intrusion.

Figure 12: Linear and nonlinear parameters as function of the macroscopic capillary pressure for Lavoux, Meule and Berea.

Figure 13: Representation of a hysteretic mesoscopic unit (a), and typical example of a P-M space density (b).

Figure 14: Influence of fluid loading on the P-M space density and on the behavior of a hysteretic mesoscopic unit.

TABLES and TABLE CAPTIONS

Table 1. Rock physical properties and dimensions.

Rock	Density (kg/m³)	Porosity (%)	Compressive Strength (MPa)	Rock Type	Geometry
Lavoux Limestone	2049	24.2	25	pelletoidal limestone 99% Calcite	Cylindrical Length: 115 cm Diameter: 5.0 cm
Meule Sandstone	2077	21.8	35	fine grained, argillaceous micaceous sandstone 74% Quartz 21% Feldspar 2% Smectite 2% Mica/Illite 1% Kaolinite	Cylindrical Length: 107.6 cm Diameter: 9.0 cm
Berea Sandstone	2186	18.6	32	fine grained sandstone 85% Quartz 8% Feldspar 5% Kaolinite 1% Smectite 1% Mica/Illite	Beam Length: 25.5 cm Width: 2.6 cm Thickness: 0.95 cm

Table 2: Fitting parameters of the water retention curves used in Eq.(7).

1) Lavoux ($w_{\text{sat}} = 251 \text{ kg/m}^3$)

k=3	l	c	n
1	0.3149	1.66E-06	3.5343
2	0.5114	5.82E-06	1.8470
3	0.1737	8.81E-06	8.4693

2) Meule ($w_{\text{sat}} = 219 \text{ kg/m}^3$)

k=3	l	c	n
1	0.0627	1.18E-07	1.7591
2	0.4583	3.02E-05	1.4392
3	0.4790	4.03E-05	8.3748

3) Berea ($w_{\text{sat}} = 186 \text{ kg/m}^3$)

k=3	l	c	n
1	0.2868	6.07E-06	1.5920
2	0.5080	4.59E-05	3.5004
3	0.2053	5.45E-05	9.8465

Figure 1: Basic elements of a Resonant Bar Experiment

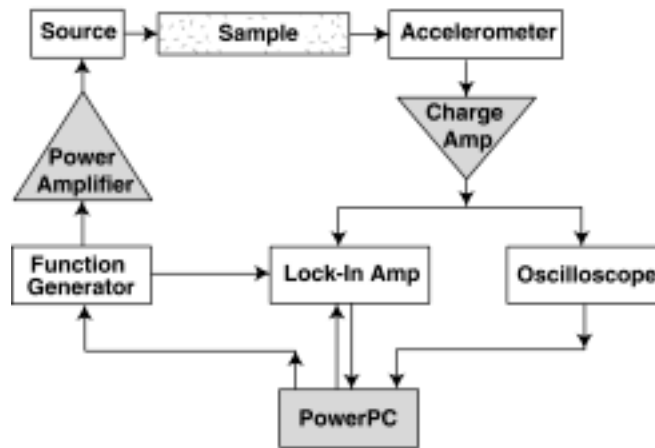


Figure 2: Young's Modulus E (a) and Inverse attenuation Q (b) as function of saturation for Lavoux limestone.

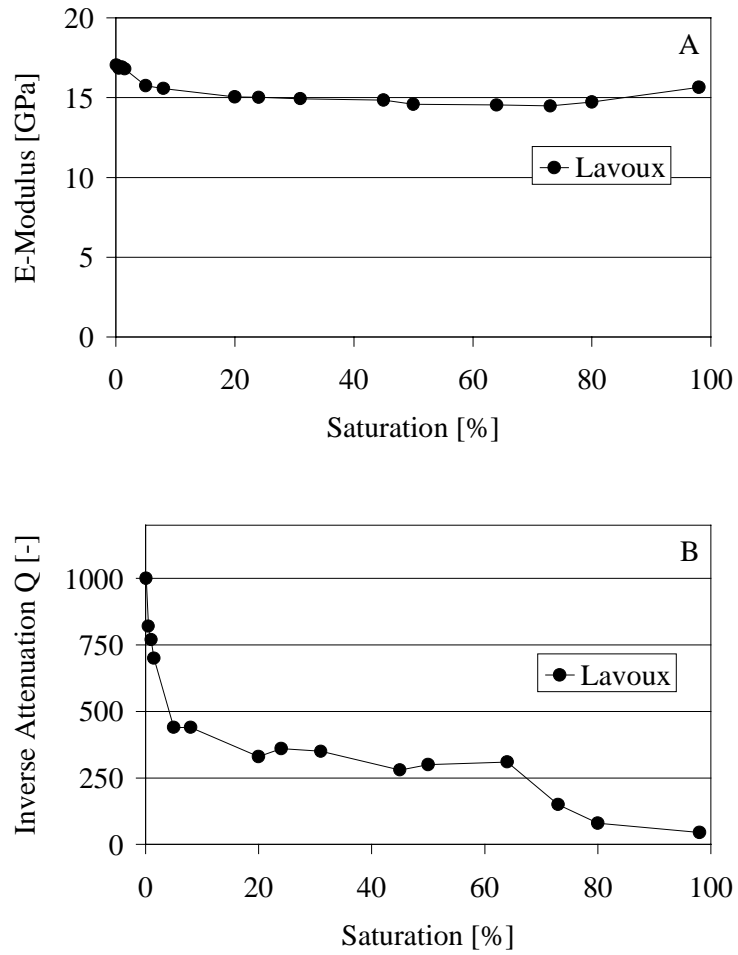


Figure 3: Changes in nonlinear response as function of saturation for Lavoux limestone.

- a) Relative Resonance Frequency Shift versus inferred strain for different saturation levels.
- b) Inferred Hysteretic Nonlinearity Coefficient α as function of saturation.

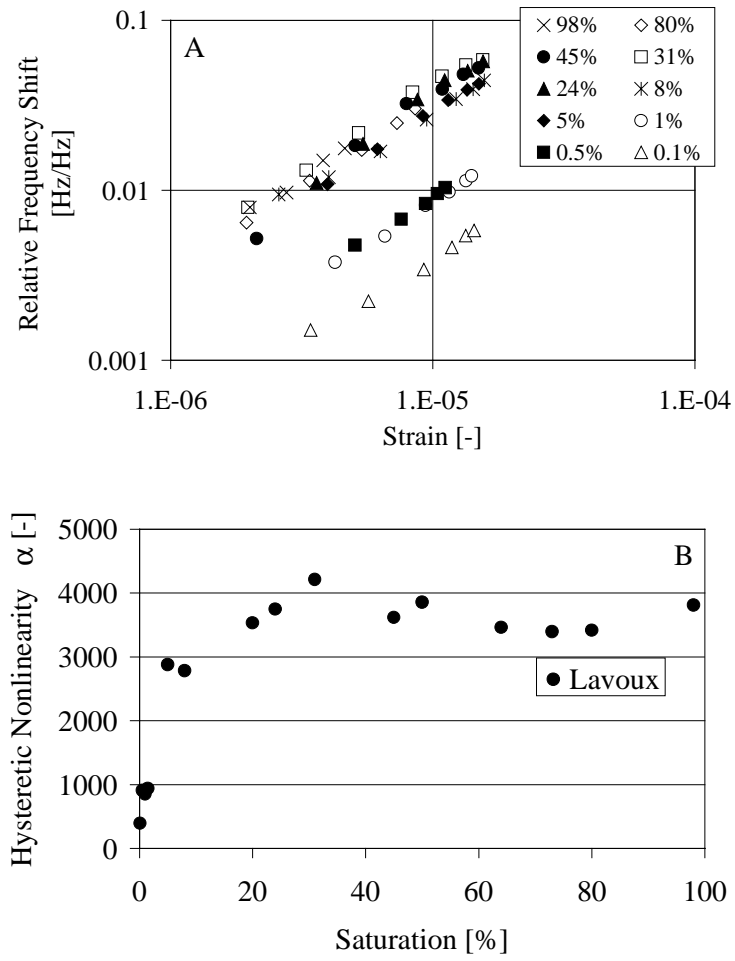


Figure 4: Young's Modulus E as function of saturation for Meule and Berea Sandstone.

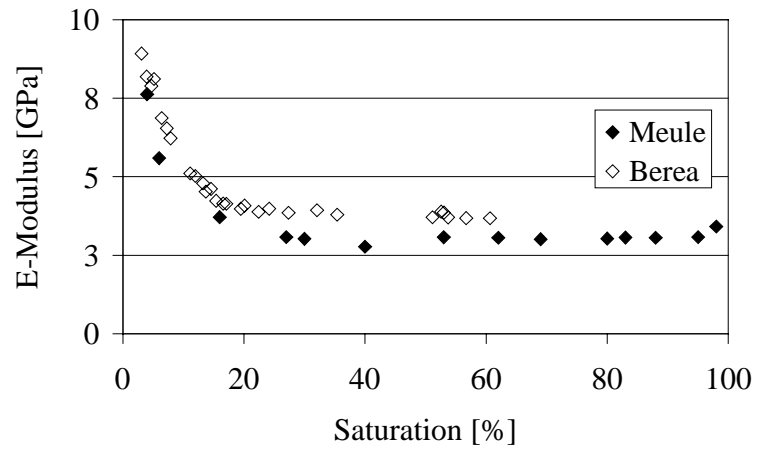


Figure 5: Inferred Hysteretic Nonlinearity Coefficient α as function of saturation for Meule and Berea sandstone.

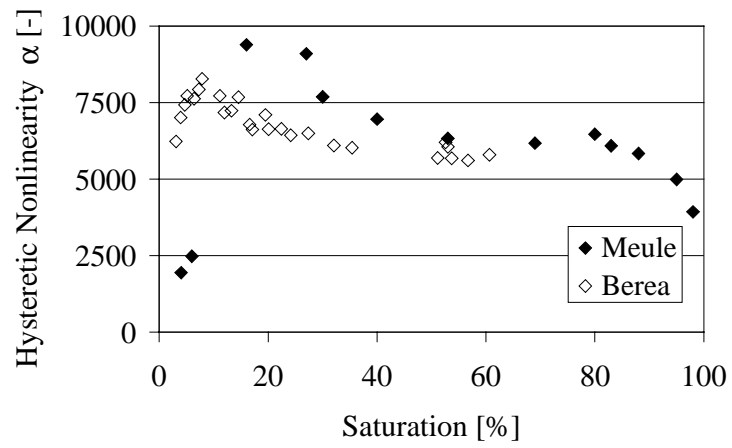


Figure 6: Quasi-static velocity measurements as function of pressure for oven-dry and 100% water saturated samples of Lavoux (a) and Meule (b) (From Zinszner et al., 1997).

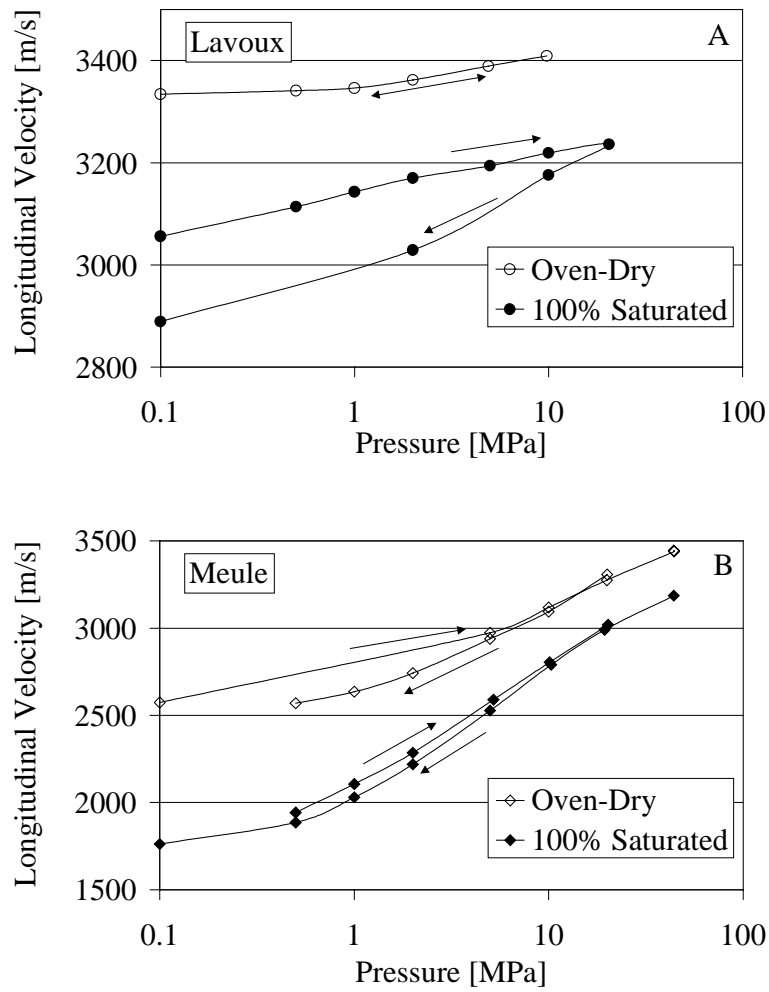


Figure7: Relative change in longitudinal velocity under 100% saturation conditions versus the relative change in longitudinal velocity under oven-dry conditions measured at the same pressure levels for Lavoux (a) and Meule(b). Due to the extreme hysteresis observed in the saturated Lavoux data, we used the mean of the interpolated velocities at each pressure level. For Lavoux a steep relation at low pressures (factor 8) is followed by moderate proportionality at high pressures (factor 4). For Meule, the dependence reveals that the nonlinearity has increased on average by a factor 2 over the entire pressure range.

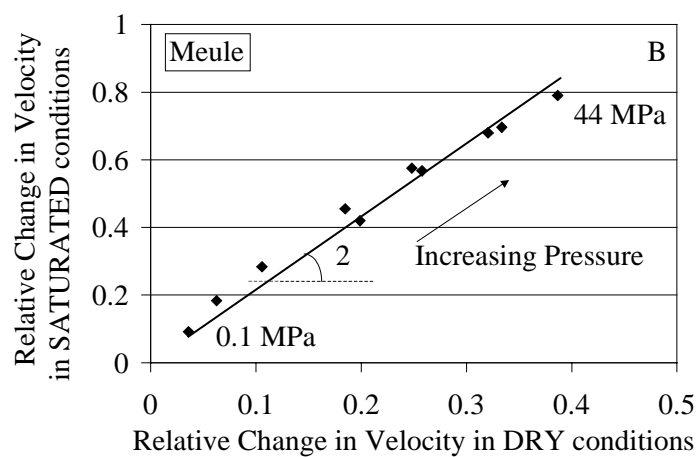
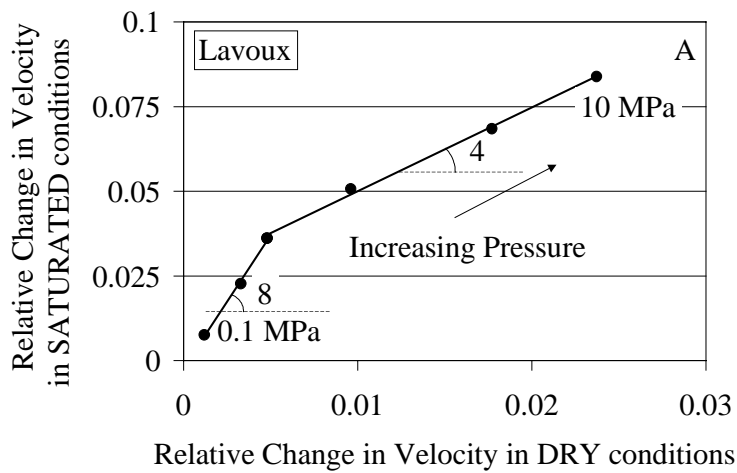


Figure 8: Sorption processes: Adsorption and Capillary Condensation

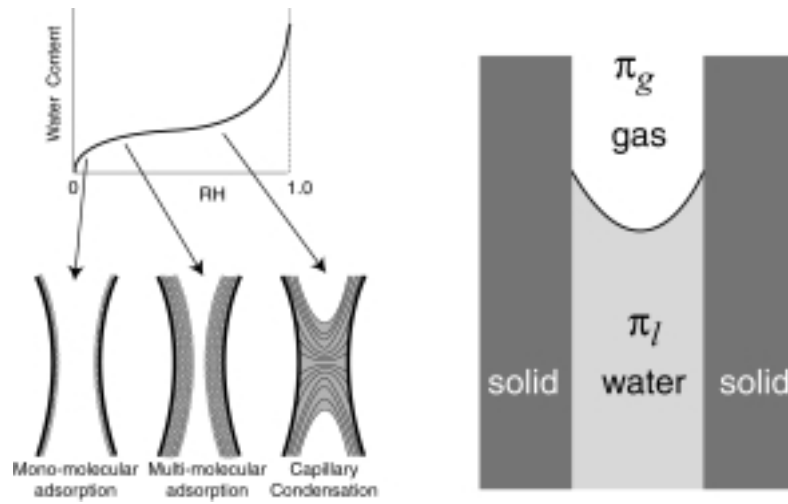


Figure 9: Moisture induced microforces: capillary (a) and swelling pressure (b) induce competing microscopic matrix reaction.

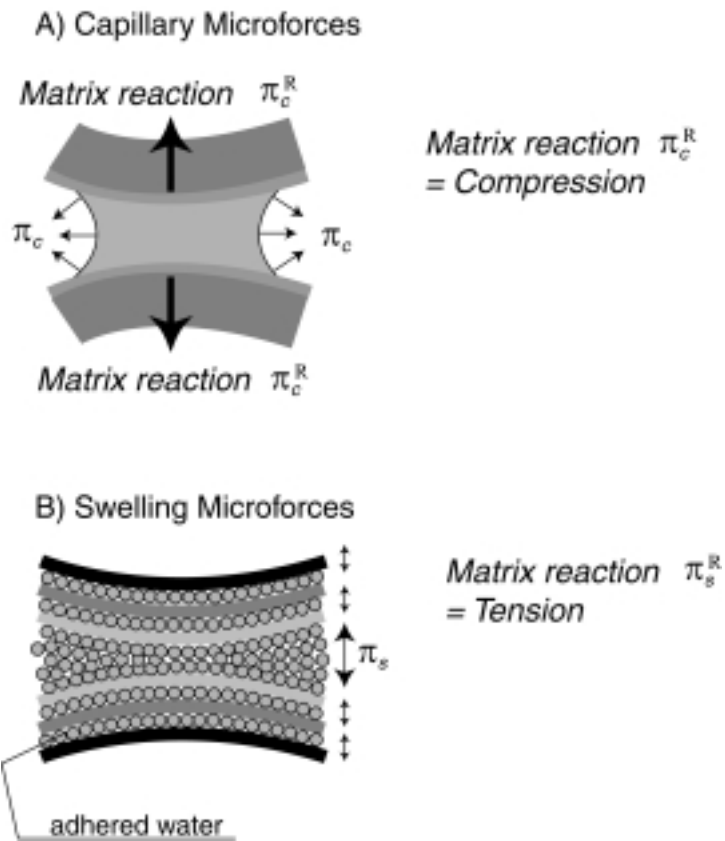


Figure 10: Solid matrix reaction due to microscopic capillary and swelling pressures. If the microscopic swelling pressure is important (e.g., in materials with clays and CSH-particles), this can lead to an extreme tensile matrix reaction near RH=1. This effect is highly exaggerated in this figure for illustrative purposes.

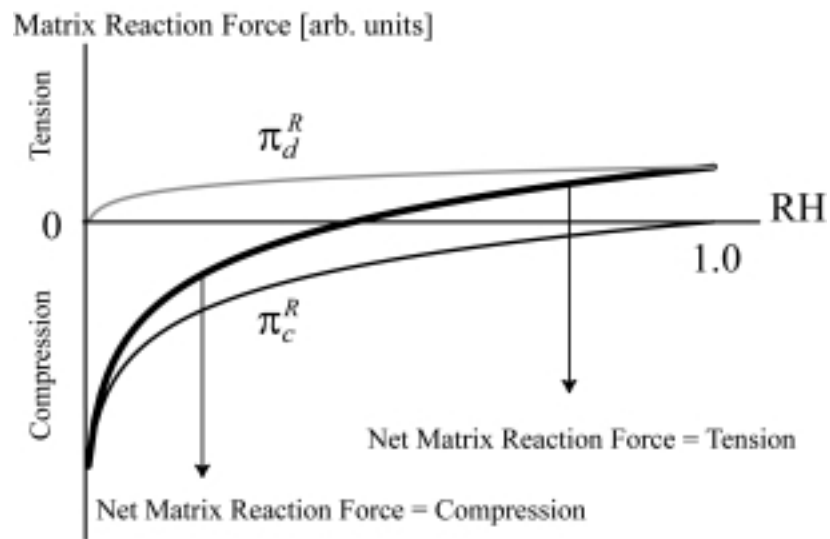


Figure 11: Capillary pressure (water retention) curves of Lavoux limestone and Meule and Berea Sandstone, measured by mercury intrusion.

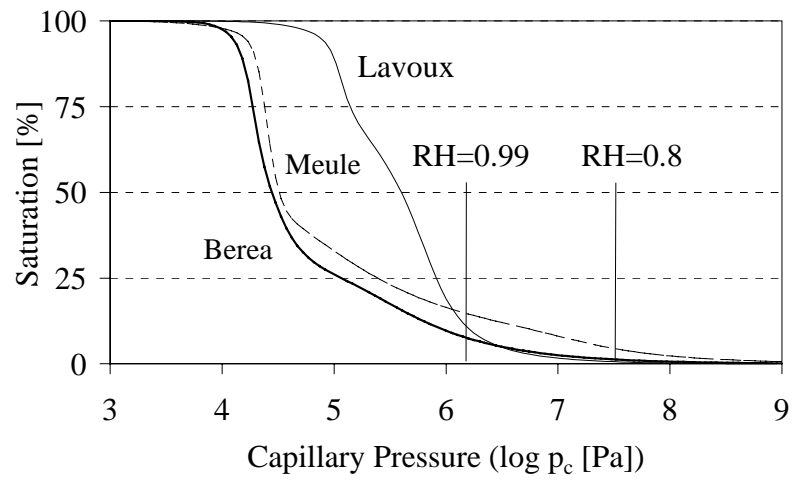


Figure 12: Linear and nonlinear parameters as function of the macroscopic capillary pressure for Lavoux, Meule and Berea.

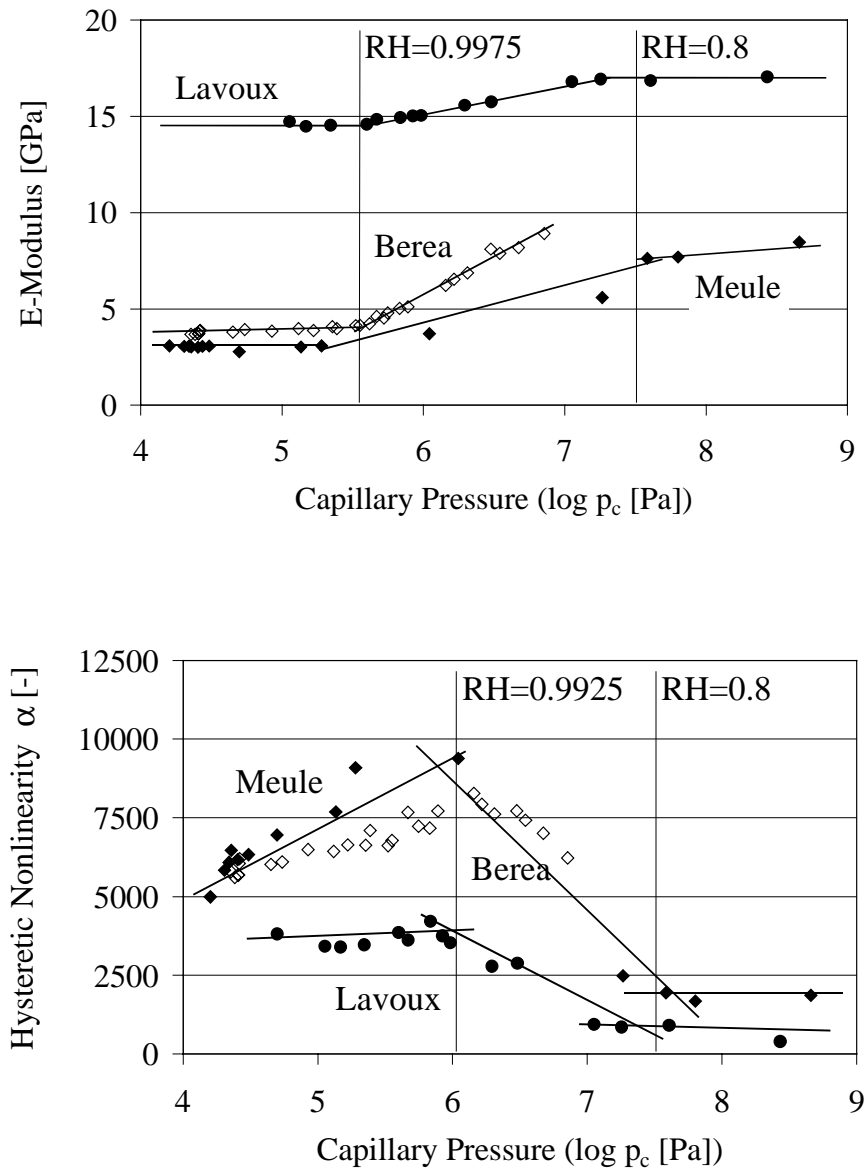
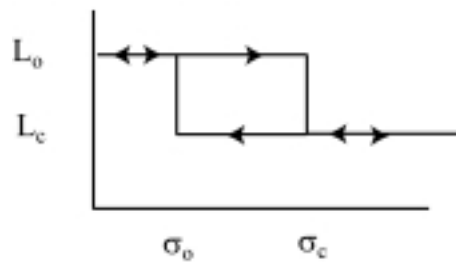


Figure 13: Representation of a hysteretic mesoscopic unit (a), and typical example of a P-M space density (b).

a) Mesoscopic Hysteretic Unit



b) PM density: signature of the material's mesoscopic unit distribution

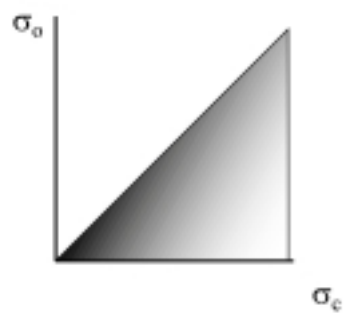
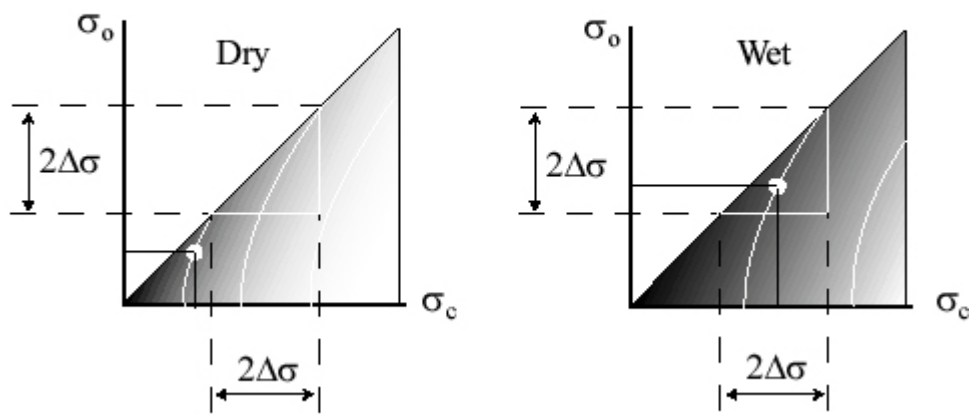


Figure 14: Influence of fluid loading on the P-M space density, and on the behavior of a hysteretic mesoscopic unit.

a) Effect on the PM density



b) Effect on the Mesoscopic Hysteretic Unit

